PERGAMON

International Journal of Multiphase Flow 26 (2000) 891–920

International Journal of Multiphase Flow

www.elsevier.com/locate/ijmulflow

Microflotation of fine particles in the presence of a bulk-insoluble surfactant

José A. Ramirez, Robert H. Davis*, Alexander Z. Zinchenko

Department of Chemical Engineering, University of Colorado, Boulder, CO 80309-0424, USA

Received 28 December 1998; received in revised form 11 June 1999

Abstract

A theoretical description of the flotation of semiBrownian spherical particles by small spherical bubbles containing a surface active substance is presented. The surfactant is considered to be insoluble in the bulk and to have small deviations in surface coverage. Collection efficiencies between the surfactant covered bubbles and the rigid particles are calculated with allowance for gravity, Brownian motion, and van der Waals attraction for a variety of bubble Péclet numbers and particle-to-bubble size ratios. The hydrodynamic problem was decomposed into axisymmetric and asymmetric parts, and pairwise hydrodynamic mobility functions were calculated for different degrees of bubble surface mobility. The effect of the adsorbed surfactant is characterized by the dimensionless surface retardation parameter, $A = MaPe_s$, a product of the Marangoni and surface Péclet numbers. $A = 0$ corresponds to a bubble with a freely mobile interface. For the limiting case of $A \to \infty$, the axisymmetric problem reduces to that of a bubble with a rigid interface. In the asymmetric problem, however, higher transversal mobilities occur for the case of $A \to \infty$ than for those of a rigid bubble. This fact results in lower collection efficiencies for $A \to \infty$ than for rigid bubbles, in some cases by as much as 80%. In general, the maximum influence of the bubble surface mobility on the collection efficiency occurs in the range where bulk convective and diffusive effects are comparable; in these cases, the collection efficiencies may vary by more than an order of magnitude for the range of possible values assumed by the surface retardation parameter.

Keywords: Flotation; Surfactants; Mobilities; Collisions; Bubbles; Particles

* Corresponding author. Tel.: +1-303-492-7314; fax: +1-303-492-4341.
E-mail address: robert.davis@colorado.edu (R.H. Davis).

0301-9322/00/$ - see front matter
PII: S0301-9322(99)00074-9

1. Introduction

In many applications in mineral engineering, environmental engineering and chemical processing, purification of aqueous streams by flotation is best carried out by the dissolved-air or electrolytic methods. These techniques generate very small bubbles with diameters in the range 20 to 100 μm, which are better suited than larger bubbles for the removal of the very fine suspended colloidal particles encountered in many of these applications (Zabel, 1984). In order to increase the hydrophobicity of the suspended matter, and thus facilitate their collection by bubbles, it is common practice to employ a surface active agent in the pulp (Gaudin, 1957). The adsorption of this surfactant on the rising bubbles and its distribution over each bubble surface affect the flotation rate.

Since the pioneering studies of Frumkin and Levich (1947) describing the retardation mechanism of an adsorbing surfactant on a single bubble rising in a liquid, numerous studies concerned with this problem have appeared in the literature. Depending on the values assumed by key physical parameters, diverse limiting situations have been identified, including a nonretarded fluid velocity profile (Wasserman and Slattery, 1969; Saville, 1973; Agrawal and Wasan, 1979; Harper, 1988), the uniformly retarded fluid velocity profile (Levich, 1962; Holbrook and LeVan, 1983), the stagnant-cap model (Griffith, 1962; Sadhal and Johnson, 1983; Cuenot et al., 1997), and the completely stagnant interface (Griffith, 1962).

The situation of interacting particles, drops, and bubbles in the presence of an adsorbed surfactant has received limited attention. The limiting case of point particles diffusing to a rising bubble whose interfacial mobility is modified by an adsorbed surfactant has been treated by Lochiel (1965). His results are applicable to conditions of Stokes flow and boundary-layer flow, the former limited to the cases of extremely high and extremely low bubble surface mobilities. Kawase and Ulbrecht (1982) extended Lochiel's analysis to rising bubbles in a non-Newtonian fluid, while Brunn and Isemin (1984) used an approximate analysis based on the integral form of the convection-diffusion equation to correlate the dimensionless mass-transfer rate to the Péclet number for a rising bubble under conditions of creeping flow. Recently, Ramirez and Davis (1999) performed an exact numerical analysis of this problem for arbitrary surface mobilities but with small deviations in surfactant coverage. Also, Blawzdziewicz et al. (1999) considered the related problem of identical surfactant-covered drops in a linear Stokes flow or in Brownian-induced motion, with allowance for van der Waals interactions. Lerner and Harper (1991) extended the stagnant-cap model to two bubbles with equal radii rising along their line of centers in Stokes flow.

In this study, we calculate the flotation rate of neutrally buoyant, spherical solid particles by spherical bubbles in an aqueous medium under the presence of a surfactant which can be considered insoluble in the bulk phase. Adsorption of this surfactant on the interface of the rising bubbles results in a non-zero tangential stress on the bubble interface, a phenomenon commonly known as the Marangoni effect. The deviation in surface coverage is assumed to be small, which corresponds to the limit of uniform retardation of the interfacial velocity (Harper, 1988). Under the assumption of negligible inertia, the motion of the bubble and suspended particle is decomposed into axisymmetrical and asymmetrical contributions. Pairwise hydrodynamic mobility functions are calculated through the methods of bispherical coordinates and multipole expansions, respectively. These mobility functions are used to calculate the

bubble-particle collection efficiencies under conditions relevant to microflotation. The effects of buoyancy, Brownian motion, and van der Waals attraction are considered.

2. Formulation of the problem

We consider a dilute dispersion of spherical bubbles of radius a_1, number density n_1, and negligible density and viscosity rising with velocity V_1^0 in an undisturbed fluid of density ρ and viscosity μ. The fluid contains small solid particles of radius a_2, number density n_2, solid density ρ_2, and sedimentation velocity V_2^0. The interfacial mobility of the rising bubble is affected by an adsorbed surfactant. Since we will be limited to the conditions typical of microflotation (spherical bubbles no larger than 50 μm in diameter rising in water at ambient temperature), the governing equations for the fluid surrounding the bubble and particle are the Stokes equations,

$$\mu\nabla^2 v = \nabla p, \tag{1a}$$

$$\nabla \cdot \boldsymbol{v} = 0. \tag{1b}$$

In the vicinity of the suspended particle, the boundary conditions necessary to specify the flow field are (i) impenetrability of the particle surface and (ii) no slip. For the case of the rising bubble, the condition of zero normal relative velocity at the surface of the bubble applies (assuming no deformation of the interface occurs for small bubbles); however, the tangential stress balance implies the existence of a finite interfacial shear stress given by (Levich, 1962)

$$\tau_t = \nabla_s \sigma, \tag{2}$$

where τ_t is the tangential stress vector and ∇_s is the surface gradient of the interfacial tension. The interfacial tension is a function of the local surfactant surface coverage: $\sigma = \sigma(\Gamma)$.

The transport of insoluble surfactant on the surface of the translating bubble at steady-state is governed by (Levich, 1962)

$$\nabla_s \cdot \left[\Gamma \boldsymbol{v}_t^* - D_s \nabla \Gamma\right] = 0, \tag{3}$$

where $\boldsymbol{v}_t^*$ is the fluid tangential velocity relative to the center of the moving bubble, D_s is the isotropic surfactant surface diffusivity, and Γ is the surfactant surface concentration. The latter may be written as $\Gamma = \Gamma_0 + \Delta\Gamma$, where Γ_0 is the average surfactant surface concentration and $\Delta\Gamma$ is the deviation from the average. The characteristic diffusive flux of surfactant along the bubble surface is then of order $D_s\Delta\Gamma/a_1$, while the convective flux is of order $V_1^0\Gamma_0$ (or less, if strong Marangoni stresses due to the surfactant concentration gradient retard the interfacial motion). Thus, the deviation in surface coverage is small compared to the average value, $\Delta\Gamma \ll \Gamma_0$, when surface diffusion is strong, $Pe_s = V_1^0 a_1/D_s \ll 1$, where Pe_s is the surface Péclet number for the bubble. The deviation in surface coverage is also small when the Marangoni stresses are strong, as shown by Cristini et al. (1998) and Blawzdziewicz et al. (1999), even if surface diffusion is weak. In this case, a Marangoni stress of order $B\Delta\Gamma/a_1$ balances the viscous stress of order $(\mu V_1^0)/a_1$ on the bubble surface, where $B = -\partial\sigma/\partial\Gamma$ is assumed constant

for small variations in surface concentration. Thus, the condition $\Delta\Gamma \ll \Gamma_0$ is met when $Ma = B\Gamma_0/\mu V_1^0 \gg 1$, where Ma is the Marangoni number, for arbitrary Pe_s. Note that $B = RT$ for nonionic surfactants at low surface coverages in the absence of long-range interactions (Levich, 1962), where R is the universal gas law constant and T is the absolute temperature. The requirement $Pe_s \ll 1$ or $Ma \gg 1$ for nearly uniform surface coverage is typically met for the small bubbles used in microflotation (Ramirez and Davis, 1999).

The tangential stress jump at the bubble interface yields the relation $\tau_t = \nabla_s\sigma = -B\nabla_s\Gamma$. Substituting this relation in Eq. (3) with $\Gamma \cong \Gamma_0$ yields

$$A\nabla_s \cdot v_t + \nabla_s \cdot \boldsymbol{\Pi}_t = 0, \tag{4}$$

where $v_t = v_t^*/V_1^0$, $\boldsymbol{\Pi}_t = (a_1\tau_t)/(\mu V_1^0)$, $A = (B\Gamma_0 a_1)/(\mu D_s) = MaPe_s$ is the surface retardation parameter, and the spatial variables have been made non-dimensional by the bubble radius, a_1. For small values of A, the surfactant has little effect on the free-slip flow along the bubble interface, whereas Marangoni stresses due to the surfactant gradient retard interfacial motion at large A.

The collision efficiency is calculated by finding the ratio between the actual flux of particles into the contact surface enclosing the bubble at $r = a_1 + a_2$, and the flux resulting when bubble-particle interactions are neglected, J_{12}^0. The former is given by (Zinchenko and Davis, 1994)

$$J_{12} = -n_1 n_2 \int_{r\to a_1+a_2} p(\boldsymbol{V}_1 - \boldsymbol{V}_2)\cdot\frac{\boldsymbol{r}}{r}\,\mathrm{d}A, \tag{5}$$

where n_1 and n_2 are the number densities of bubbles and particles at a given time of size a_1 and a_2, $p(\boldsymbol{r})$ is the pair distribution function (Batchelor, 1982), $\boldsymbol{V}_1(\boldsymbol{r})$ and $\boldsymbol{V}_2(\boldsymbol{r})$ are the velocities of the interacting bubble and particle, respectively, and $\boldsymbol{r}$ is the vector connecting the centers of the bubble and particle. The collection efficiency is then calculated as

$$E_{12} = \frac{J_{12}}{J_{12}^0} = \frac{J_{12}}{n_1 n_2\left(V_1^0 - V_2^0\right)\pi(a_1+a_2)^2}. \tag{6}$$

The pair distribution function, $p(\boldsymbol{r})$, is obtained by solving the Fokker–Planck equation:

$$\nabla\cdot\left[p(\boldsymbol{V}_1 - \boldsymbol{V}_2)\right] = 0. \tag{7}$$

In order to describe the hydrodynamic interactions between the bubble and particle, we write their relative velocity as (Batchelor, 1982)

$$\boldsymbol{V}_1(\boldsymbol{r}) - \boldsymbol{V}_2(\boldsymbol{r}) = \left(\boldsymbol{V}_1^0 - \boldsymbol{V}_2^0\right)\cdot\left[\frac{\boldsymbol{rr}}{r^2}L(s) + \left(\boldsymbol{I} - \frac{\boldsymbol{rr}}{r^2}\right)M(s)\right] - \frac{D_{12}^0}{kT}\cdot\left[\frac{\boldsymbol{rr}}{r^2}G(s) + \left(\boldsymbol{I} - \frac{\boldsymbol{rr}}{r^2}\right)H(s)\right]$$
$$\cdot\nabla\Phi_{12}(\boldsymbol{r})$$

$$-D_{12}^0\left[\frac{\boldsymbol{rr}}{r^2}G(s) + \left(\boldsymbol{I} - \frac{\boldsymbol{rr}}{r^2}\right)H(s)\right]\cdot\nabla(\ln p(\boldsymbol{r})), \tag{8}$$

where $s = 2r/(a_1 + a_2)$, $\boldsymbol{I}$ is the unit second order tensor, kT is the product of the Boltzman constant and the absolute temperature, T, and Φ_{12} is the interparticle potential. The velocity of an isolated bubble due to buoyancy is given by Levich (1962), considering the effects of a bulk-insoluble surfactant on its surface:

$$\boldsymbol{V}_1^0 = -\frac{2}{9\mu}\rho a_1^2 \frac{A+3}{A+2}\boldsymbol{g}, \tag{9}$$

where $\boldsymbol{g}$ is the gravity acceleration vector. The sedimentation velocity of an isolated particle is given by Stokes law: $\boldsymbol{V}_2^0 = 2(\rho_2 - \rho)a_2^2\boldsymbol{g}/(9\mu)$, but it is assumed that the particle is small compared to the bubble and/or neutrally buoyant, so that $V_2^0 \ll V_1^0$.

The relative diffusivity when the bubble and particle are widely separated and non-interacting is (Batchelor, 1982)

$$D_{12}^0 = D_1^0 + D_2^0 = \frac{kT(3+A)}{6\pi\mu a_1(2+A)} + \frac{kT}{6\pi\mu a_2}. \tag{10}$$

3. Method of solution

In order to solve Eq. (7), we first write Eq. (8) in spherical coordinates (Zhang and Davis, 1991):

$$\begin{aligned}\frac{\mathbf{V}_1(\mathbf{r}) - \mathbf{V}_2(\mathbf{r})}{V_1^0 - V_2^0} &= -L\cos\theta\boldsymbol{e}_r + M\sin\theta\boldsymbol{e}_\theta - \frac{1}{Q_{12}}G\frac{\mathrm{d}\phi}{\mathrm{d}s}\boldsymbol{e}_r \\ &\quad - \frac{1}{Pe_{12}}\left[G\frac{\partial(\ln p)}{\partial s}\boldsymbol{e}_r + \frac{H}{s}\frac{\partial(\ln p)}{\partial\phi}\boldsymbol{e}_\theta\right],\end{aligned} \tag{11}$$

where $\boldsymbol{e}_r$ and $\boldsymbol{e}_\theta$ are the unit vectors along and normal to the line of centers, respectively, and θ is the angle defined by $g\cos\theta = -\boldsymbol{g}\cdot\boldsymbol{e}_r$. The relative Péclet number, Pe_{12}, provides a measure of the relative importance between gravitational motion and Brownian diffusion, and the parameter Q_{12} is a ratio of gravitational and van der Waals contributions:

$$Pe_{12} = \frac{(a_1 + a_2)\left(V_1^0 - V_2^0\right)}{2D_{12}^0}, \qquad Q_{12} = \frac{kTPe_{12}}{A_{\mathrm{H}}}. \tag{12}$$

Substitution of Eq. (11) into Eq. (7) yields, after neglecting the contribution of transversal diffusion (Zinchenko and Davis, 1994),

$$\frac{\partial}{\partial s}\left[s^2 pLu + \frac{Gs^2 p\hat{A}}{Pe_{12}}\frac{\mathrm{d}\phi}{\mathrm{d}s} + \frac{Gs^2}{Pe_{12}}\frac{\partial p}{\partial s}\right] = Ms\frac{\partial\left[p(u^2-1)\right]}{\partial u}. \tag{13}$$

Here, $u = \cos\theta$, the dimensionless Hamaker constant, $\hat{A}$, is normalized by kT, and the

dimensionless interparticle force potential is given by $\phi = \Phi_{12}/A_H$ (where Φ_{12} is the force potential and A_H is the composite Hamaker constant).

The neglect of the contribution of diffusion in the transversal direction is commonly referred to as the parabolic approximation (Zinchenko and Davis, 1994). For small relative Péclet numbers ($Pe_{12} \ll 1$), Brownian diffusion is dominant and the pair-distribution, p, is radially symmetric (depending only on s and not on θ). Then, transverse diffusion in the angular direction is negligible. For the opposite limit of $Pe_{12} \gg 1$, for which gravitational motion is dominant, the pair-distribution function is also radially symmetric (Batchelor, 1982). Although this radial symmetry does not hold for intermediate Pclet numbers, the global error in the collection efficiency resulting from the neglect of transverse diffusion is expected to be small. Indeed, as shown by Zinchenko and Davis (1994) for coalescence of drops of the same fluid dispersed in a second fluid, the global contribution of the transversal diffusion term is always insignificant (although local contributions exist), with errors in the coalescence rate not exceeding 2–3% when the whole range of relative Péclet numbers is considered.

The parabolic differential equation is solved by expanding the solution for $p(s,u)$ in powers of $u-1$ (assuming regularity at $u=1$) for a given value of Pe_{12}, instead of finite-difference marching from $u=1$, and then successively finding the coefficients of a sufficient number of terms by substituting this power expansion into Eq. (13). In the radial direction, the same finite-difference scheme as in Zinchenko and Davis (1994) is used. The cutoff distance was set at $s_\infty = 25$, which allows us to cover the whole range from moderate to large Pe_{12}.

The hydrodynamic mobility coefficients are calculated a priori as functions of the interparticle distance, s, for use in the finite-difference scheme for the radial direction. Due to the linearity of the Stokes equations, the hydrodynamic problem may be treated by separately considering the instantaneous bubble-particle motion along their line of centers (axisymmetric problem) and perpendicular to the their line of centers (asymmetric motion). The first problem is solved in a resistance formulation through the technique of bispherical coordinates (Stimson and Jefferey, 1926), while the latter was approached through the method of multipole expansions, following the technique outlined by Zinchenko (1982). Even though the method of multipole expansions is computationally much simpler than that of bispherical coordinates, it becomes quite inefficient for the axisymmetric problem when the separation is small at extreme particle-to-bubble size ratios and very low bubble surface mobilities, necessitating a very large number of terms in the expansion before convergence is achieved. This problem does not occur for the asymmetric case, since, as will be seen later, surface sliding occurs even in the case of high values of A, which results in reasonable convergence rates. A detailed description of both methods can be found in Appendices A and B for the calculation of the axisymmetric mobility coefficients (L and G) and the asymmetric mobility functions (M and H), respectively.

4. Results and discussion

In order to better understand the effect of the adsorbed surfactant on the overall collection efficiencies, it is useful to study the behavior of the pair-wise mobility functions at varying degrees of surface mobility. In the discussion in the following paragraphs, the terms completely mobile and rigid will be used in reference to a bubble whose interface is free of surfactant and

has no tangential stress and one whose interface is completely immobile and has no tangential velocity relative to the center of the bubble, respectively.

4.1. Relative mobility functions for gravitational motion

Fig. 1 shows the dimensionless relative velocity along the line of centers for motion induced by gravity, for three values of the particle-to-bubble size ratio, $\lambda = a_2/a_1$, representative of the range typically encountered in microflotation. As expected, the relative mobility decreases with decreasing separation and increasing values of the retardation parameter, due to increased hydrodynamic interactions. As the dimension of the particle becomes comparable to that of the bubble (see Fig. 1(a)), the dependence of the relative mobility function on the surface retardation weakens, tending to completely mobile behavior at sufficiently small dimensionless gaps for any finite A. This is due to the lubrication flow in the narrow gap separating the particle and bubble being able to overcome the Marangoni stresses and cause the interface to flow (Cristini et al., 1998). For smaller particles (see Fig. 1(b) and (c)), the relative velocity with respect to the rising bubble is dictated mainly by the flow field surrounding the bubble, as the effect of the particle on this flow field diminishes with decreasing particle size. The dependence of the relative mobility function with A is then mainly the result of the changing flow field around the rising bubble due to the change in boundary condition with varying A; in this case, the lubrication flow does not dominate until extremely small separations; thus, the relative mobility functions do not exhibit the tendency to asymptote towards the completely mobile solution in the range of practical separations.

The dimensionless relative velocity for gravity-induced motion in the direction perpendicular to the line of centers is shown in Fig. 2. As expected, the transverse relative mobility function tends to a constant value as $s - 2 \rightarrow 0$. However, the higher values of the mobility for finite values of A (with respect to those for the case of a rigid bubble) point to the existence of lower tangential stresses at the bubble surface, consonant with the more relaxed velocity profiles that result from interfacial motion. Unlike for axisymmetric motion, the limit $A \rightarrow \infty$ does not correspond to rigid spheres. Instead, the surfactant-covered bubble slides past the rigid particle with reduced resistance, similar to the finding of Blawzdziewicz et al. (1999) for two surfactant-covered bubbles. This effect becomes smaller as the particle-to-bubble size ratio is reduced.

4.2. Relative mobility functions for Brownian motion

Fig. 3 shows the dimensionless relative velocity along the line of centers for motion induced by Brownian diffusion or by an interparticle force. As for gravitational motion, the no-slip condition on the surface of the rigid particle results in the relative mobility function tending to zero as the gap decreases. However, the effect of surface retardation on the relative mobility is weaker than for gravitational motion, particularly at smaller gap separations.

The relative mobility function normal to the line of centers for Brownian motion is shown in Fig. 4 and exhibits unusual behavior, including values greater than unity. A small particle in Brownian motion has a high velocity relative to a larger bubble. As the particle approaches the bubble, this velocity is retarded if the bubble surface is rigid. However, if the bubble surface is mobile, then the particle experiences less resistance when it is close to the bubble surface than

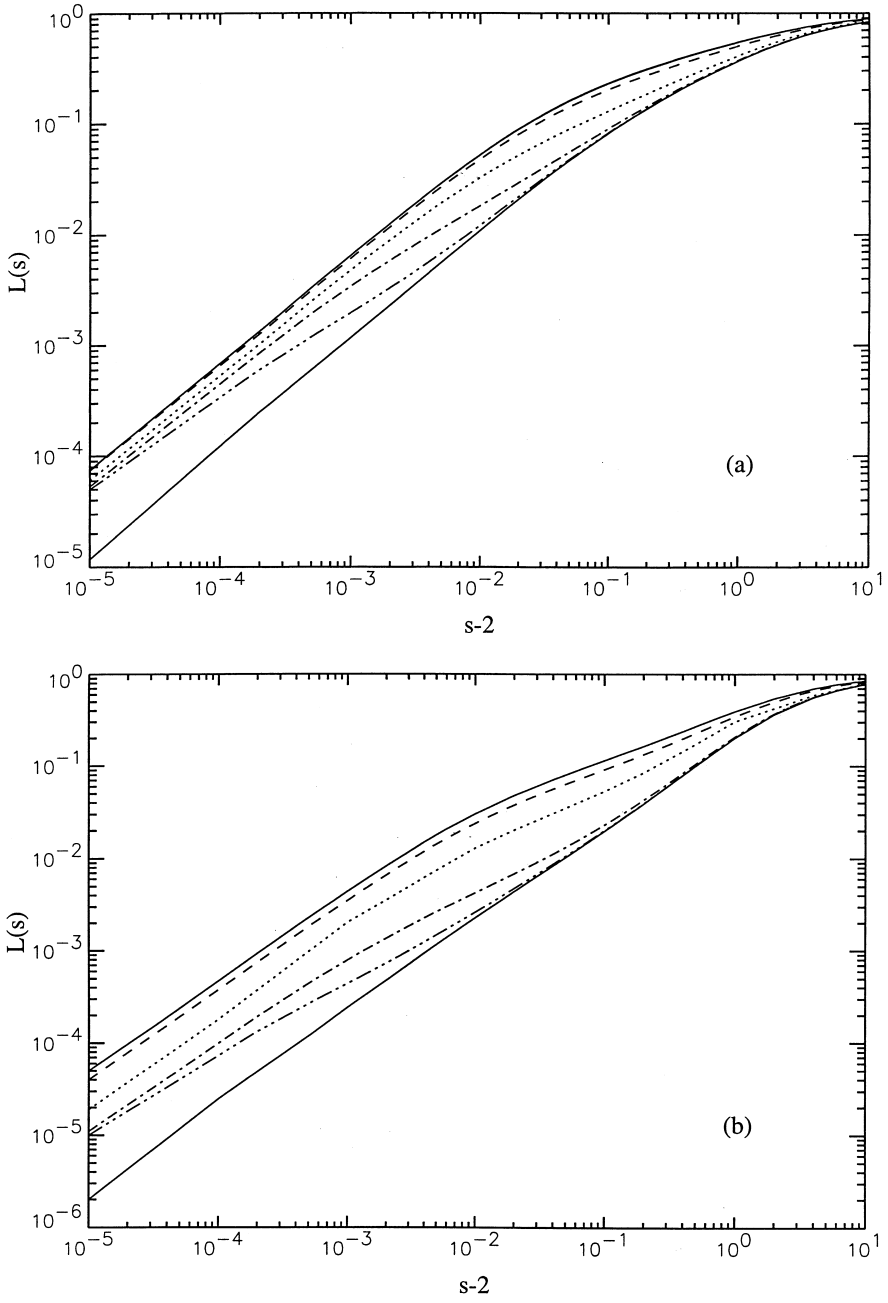

Fig. 1. The axisymmetric mobility function for gravitational motion versus the dimensionless interparticle separation for particle-to-bubble size ratios of (a) $\lambda = 0.5$, (b) $\lambda = 0.1$ and (c) $\lambda = 0.02$. Results shown are for $A = 0$ (upper solid line), $A = 0.1$ (coincident with line for $A = 0$), $A = 1.0$ (dashed line), $A = 10.0$ (dotted line), $A = 100$ (dot-dashed line) and $A = 10^3$ (dot-dot-dashed line). The lower solid line represents the results for $A \to \infty$ and is coincident with the results for two approaching solid spheres.

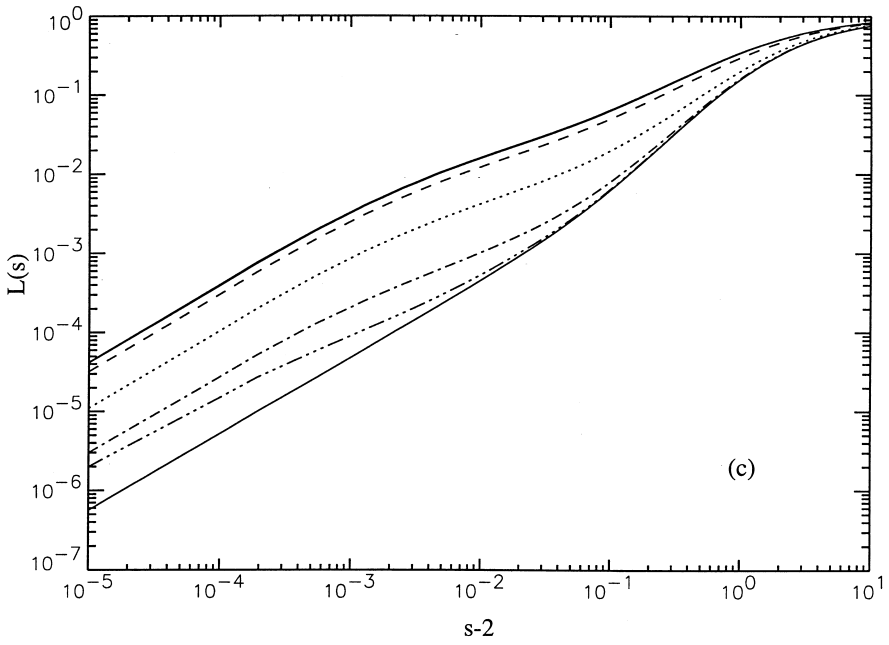

Fig. 1 (*continued*)

when it is isolated in the bulk fluid. This effect yields increased transverse relative mobilities for $\lambda = 0.1$ and 0.02 (Fig. 4(b) and (c)) but not for larger particles ($\lambda = 0.5$, Fig. 4(a)).

4.3. Collection efficiencies

The parabolized versions of Eqs. (7) and (8) (which involve neglecting the contribution of transverse diffusion) were solved numerically using an algorithm developed by Zinchenko and Davis (1994). All calculations account for retarded van der Waals attractive forces between the bubble and particle (Schenkel and Kitchener, 1960; Ho and Higuchi, 1968). A typical value for the Hamaker constant equal to kT was employed (Loewenberg and Davis, 1994), where k is the Boltzmann constant and T is the absolute temperature, and the London retardation wavelength was 0.1 μm. It is assumed that the surfactant is nonionic and that repulsive forces between the particle and bubble are negligible. The calculations presented in this section are based on an air bubble in water at room temperature ($T = 298$ K), so that the internal viscosity of the bubble may be neglected. The suspended particle is assumed to be rigid, and to be sufficiently small or neutrally buoyant so that its gravitational motion is negligible.

Figs. 5–7 show the collection efficiency for different values of the parameter A and three fixed bubble Péclet numbers of $Pe = a_1 V_1^0 / D_1 = 5 \times 10^3$, 2.5×10^5, and 4×10^6 (corresponding to bubbles of approximate diameters of 10, 25 and 50 μm, respectively, typical of

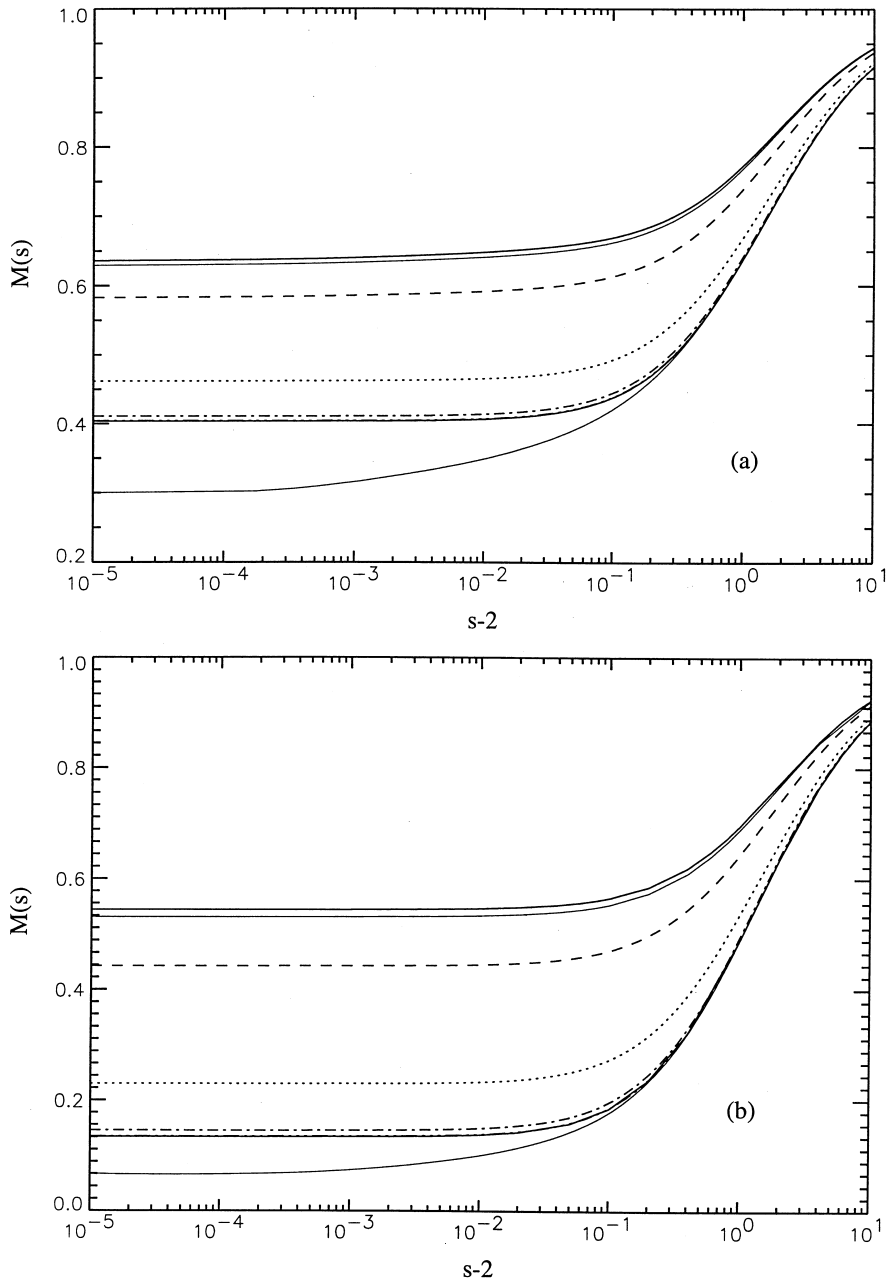

Fig. 2. The asymmetric mobility function for gravitation motion versus dimensionless interparticle separation for particle-to-bubble size ratios of (a) $\lambda = 0.5$, (b) $\lambda = 0.1$and (c) $\lambda = 0.02$. Results shown are for $A = 0$ (upper solid line), $A = 0.1$ (thin solid line below $A = 0$), $A = 1.0$ (dashed line), $A = 10.0$ (dotted line), $A = 100$ (dot-dashed line) and $A = 10^3$ (dot-dot-dashed line). The lower thin solid line represents the results for two approaching solid spheres; the solid line above it represents the results for $A \to \infty$.

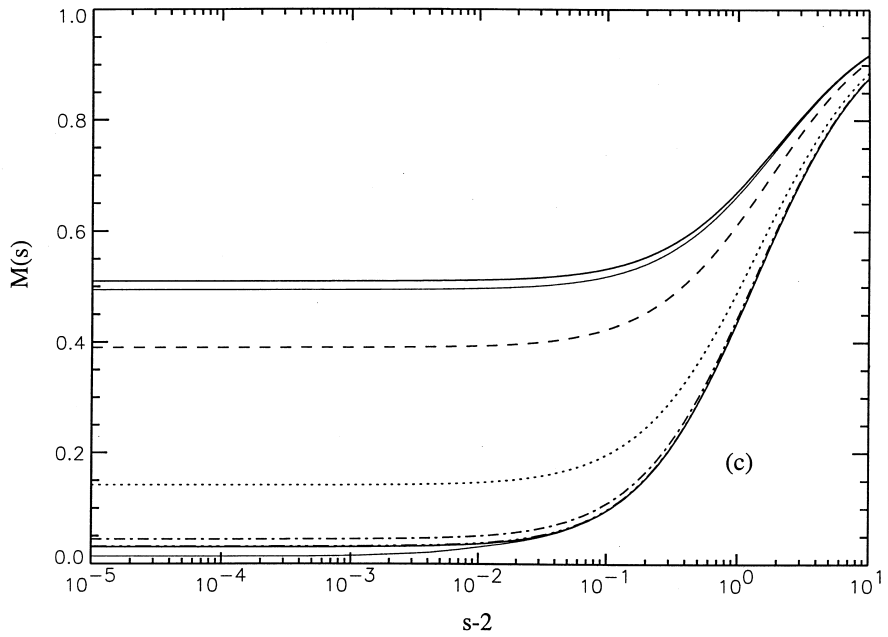

Fig. 2 (*continued*)

microflotation applications), as a function of the particle-to-bubble size ratio. Included are the results for bubbles with clean interfaces and with rigid interfaces. In all cases, bubbles with completely mobile interfaces have the highest collection efficiencies. The collection efficiency is then reduced with increasing surface retardation, since the reduced mobility of the interface provides greater resistance to the fluid being squeezed out from the region separating the approaching particles and bubble. The collection efficiencies for $A \rightarrow \infty$ are slightly lower than those for a rigid bubble, because the transverse relative mobility function $M(s)$ is higher for near contact in the former case, and the particle and bubble then move more quickly past each other.

At large size ratios, the particles (as well as the bubbles) are nonBrownian, and excellent agreement with the convective trajectory analysis is obtained. As the relative particle size is decreased, the collection efficiency decreases as the smaller particles tend to follow the streamlines and be swept around the rising bubbles. A minimum in the collection efficiency then occurs, since the Brownian motion of the particles becomes important for sufficiently small particles and increases the collision rate with further reductions in particle size. Yang et al. (1995) also predicted a minimum in the collection efficiency versus size ratio, using an approximate additivity model of particle capture by Brownian diffusion and interception acting independently. The particle-to-bubble size ratio which minimizes the collection efficiency shifts to smaller values with increasing bubble size (or Péclet number), since relatively smaller particles are required for Brownian effects to compete with convective effects. At sufficiently small particle-to-bubble size ratios, the

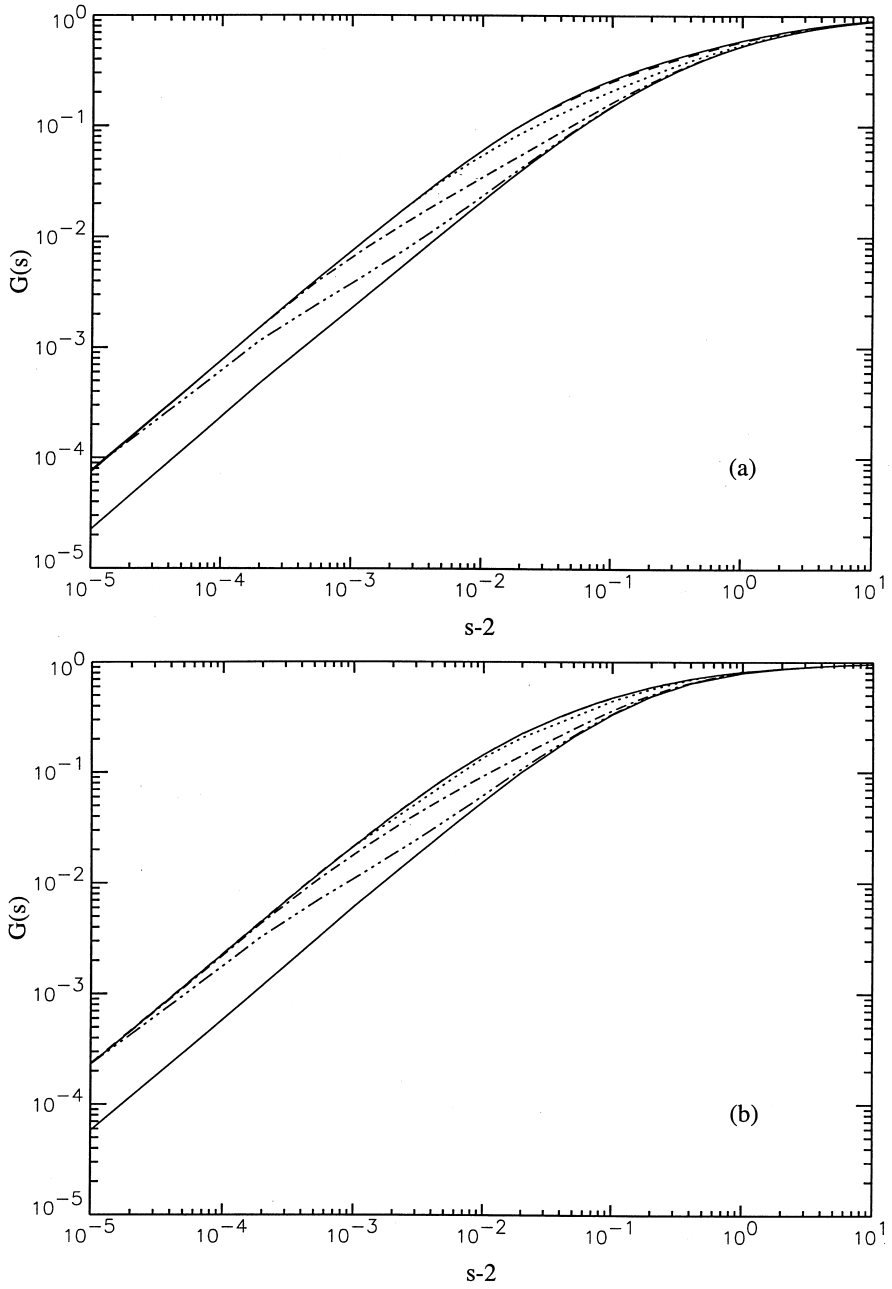

Fig. 3. The axisymmetric mobility function for Brownian diffusion versus the dimensionless interparticle separation for particle-to-bubble size ratios of (a) $\lambda = 0.5$ (a), (b) $\lambda = 0.1$ and (c) $\lambda = 0.02$. Results shown are for $A = 0$ (upper solid line), $A = 0.1$ (coincident with line of $A = 0$), $A = 1.0$ (dashed line, coincident with the previous two curves in (b) and (c)), $A = 10.0$ (dotted line), $A = 100$ (dot-dashed line) and $A = 10^3$ (dot-dot-dashed line). The lower solid line represents the results for $A \rightarrow \infty$ and is coincident with the results for two approaching solid spheres.

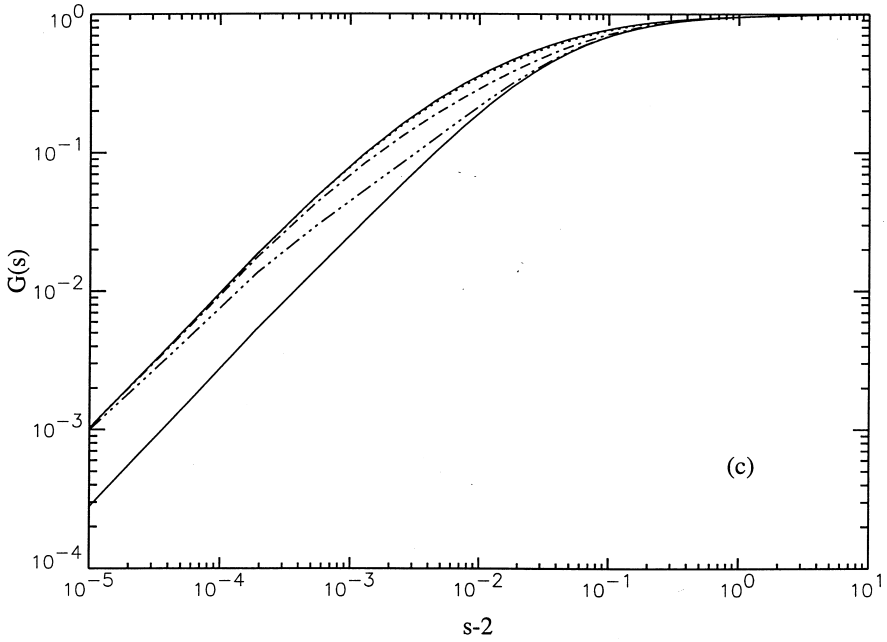

Fig. 3 (*continued*)

effect of surfactants on the collection efficiency is reduced, because Brownian motion of the solid particle becomes dominant and the velocity profile of the fluid surrounding the bubble has a weaker role.

Included in Figs. 5 and 6 are the collection efficiencies calculated from solving the convection-diffusion equation for the mass transfer of point particles diffusing to a rising bubble with surfactant on its surface (Ramirez and Davis, 1999). The mass-transfer solution slightly overpredicts the collection efficiencies, even for the case of very small suspended particles of the order of 0.1 μm in diameter (e.g., $\lambda = 0.01$ in Fig. 5). Hydrodynamic interactions retard the motion of these small but finite particles toward the bubble surfaces, so that the collection efficiency is reduced from the point-particle limit.

Figs. 8–10 display the collection efficiencies for fixed particle-to-bubble size ratios of $\lambda = 0.02$, 0.1, and 0.5, respectively, in the range of bubble Péclet numbers of relevance to microflotation (Loewenberg and Davis, 1994; Ramirez et al., 1999). The collection efficiency decreases with increasing bubble size or Péclet number in all cases, since the contributions due to Brownian diffusion and van der Waals attraction become weaker. As in the previous results, the collection efficiency also decreases with increasing surface retardation, and its values for $A \gg 1$ are below those for rigid bubbles of the same size. Surfactant effects are weakest for relatively small particles sizes (Fig. 8) and small bubble sizes (small Pe), since the Brownian motion of the particle is then dominant over convective motion due to the rising bubble. In

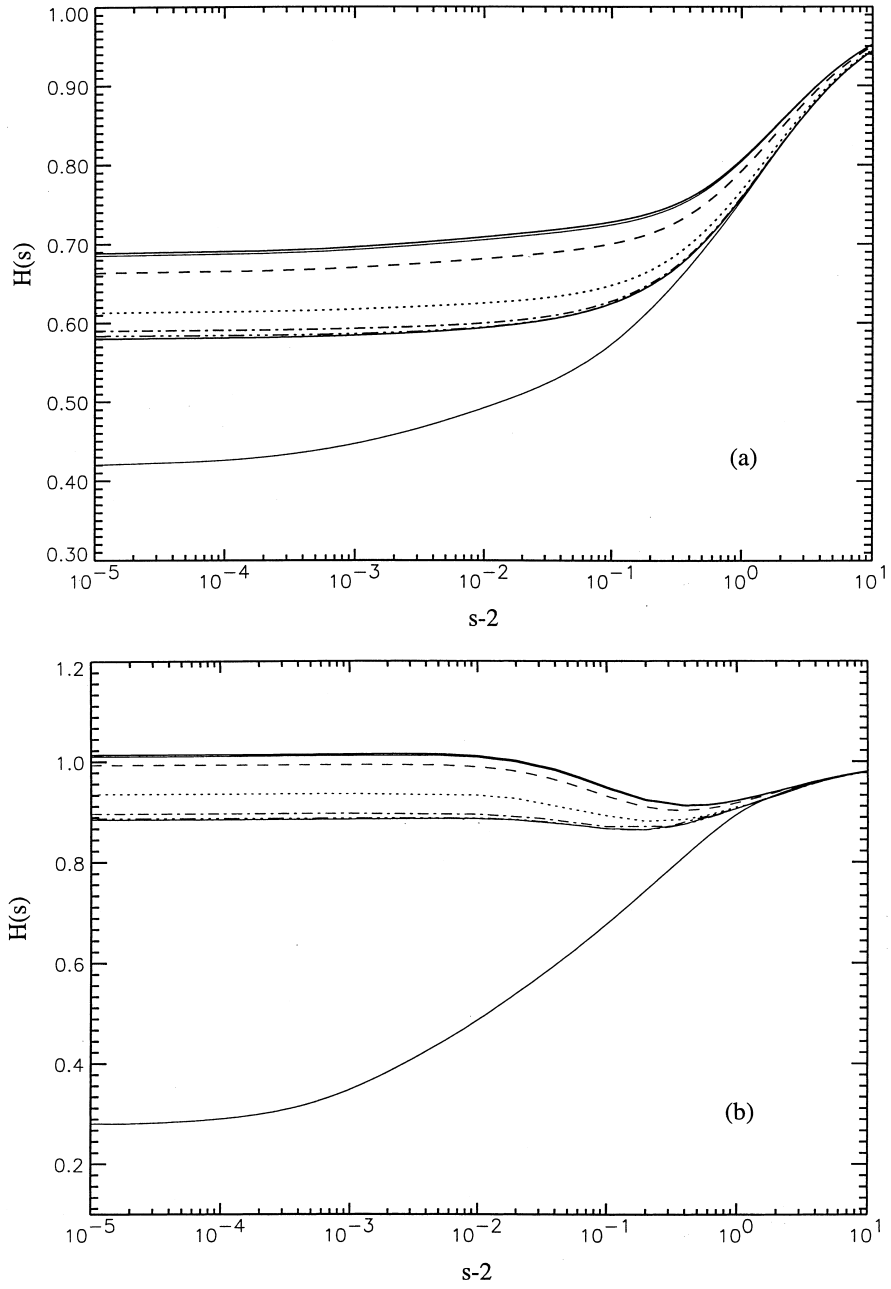

Fig. 4. The asymmetric mobility function for Brownian diffusion versus the dimensionless interparticle separation for particle-to-bubble size ratios of (a) $\lambda = 0.5$, (b) $\lambda = 0.1$ and (c) $\lambda = 0.02$. Results shown are for $A = 0$ (upper solid line), $A = 0.1$ (thin solid line below $A = 0$, coincidence occurs in (c)), $A = 1.0$ (dashed line), $A = 10.0$ (dotted line), $A = 100$ (dot-dashed line) and $A = 10^3$ (dot-dot-dashed line). The lower thin solid line represents the results for two approaching solid spheres; the solid line above it represents the results for $A \to \infty$.

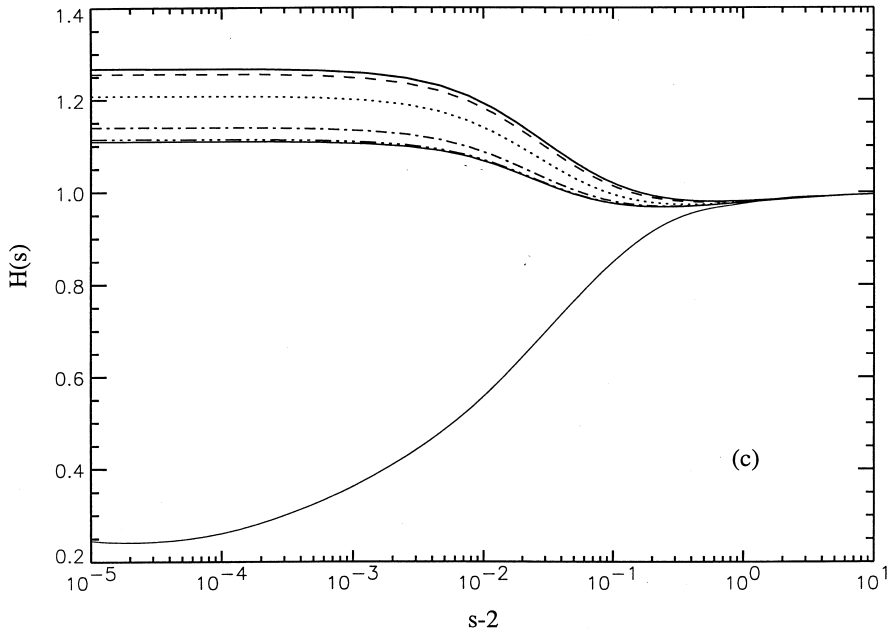

Fig. 4 (*continued*)

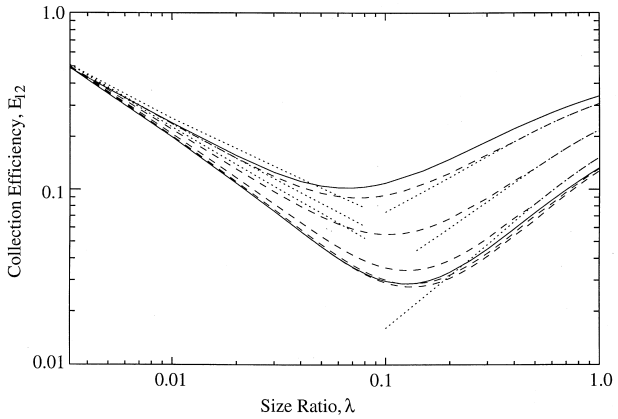

Fig. 5. Collection efficiency as a function of the particle to bubble size ratio at a fixed bubble Péclet number of $Pe = 5 \times 10^3$. The upper solid line is for a bubble with a free interface ($A = 0$), and the lower solid line is for a bubble with a rigid interface. The dashed lines are for $A = 1$, 10, 100, 1000, and ∞ (top to bottom). The dotted lines on the right-hand side are the results of trajectory calculations in the absence of Brownian diffusion for $A = 1$, 10, and 100 (top to bottom), while the dotted lines on the left-hand side are the point-particle mass-transfer solution for $A = 1$, 10, 100 (top to bottom).

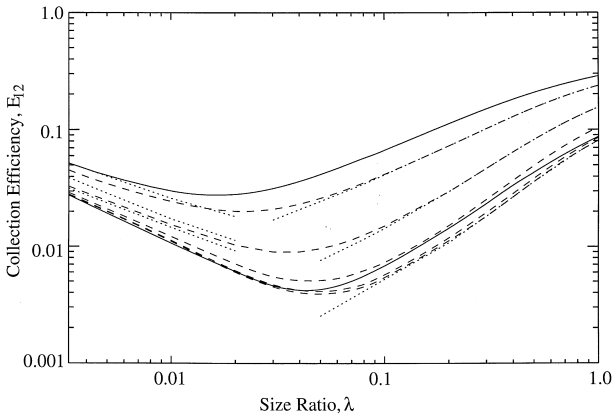

Fig. 6. Collection efficiency as a function of the particle-to-bubble size ratio at a fixed bubble Péclet number of $Pe = 2.5 \times 10^5$. The upper solid line is for a bubble with a free interface ($A = 0$), and the lower solid line is for a bubble with a rigid interface. The dashed lines are for $A = 2.5$, 25, 250, 2500, and ∞ (top to bottom). The dotted lines on the right-hand side are the results of trajectory calculations in the absence of Brownian diffusion for $A = 2.5$, 25, and ∞ (top to bottom), while the dotted lines on the left-hand side are the point-particle mass-transfer solution for $A = 2.5$, 25, 250 (top to bottom).

contrast, surfactant effects are very strong in the convection-dominant region, with the values of the collection efficiency decreasing nearly 10-fold from those for $A = 0$ to those for $A \to \infty$ for $Pe = 10^7$ (corresponding to a bubble diameter in water of about 60 μm, which is near the upper limit for Stokes motion).

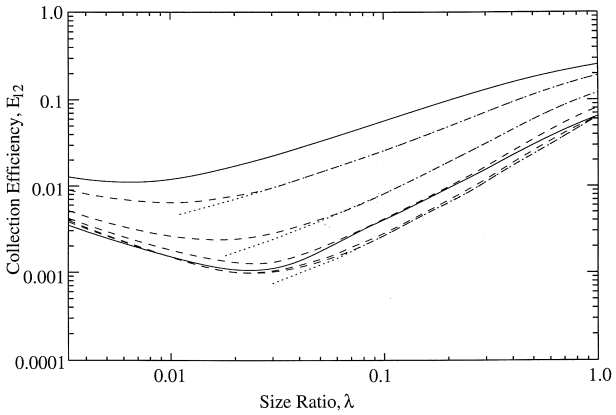

Fig. 7. Collection efficiency as a function of the particle-to-bubble size ratio at a fixed bubble Péclet number of $Pe = 4 \times 10^6$. The upper solid line is for a bubble with a free interface ($A = 0$), and the lower solid line is for a bubble with a rigid interface. The dashed lines are for $A = 5$, 50, 500, 5000, and ∞ (top to bottom). The dotted lines on the right-hand side are the results of trajectory calculations in the absence of Brownian diffusion for $A = 5$, 50, and ∞ (top to bottom).

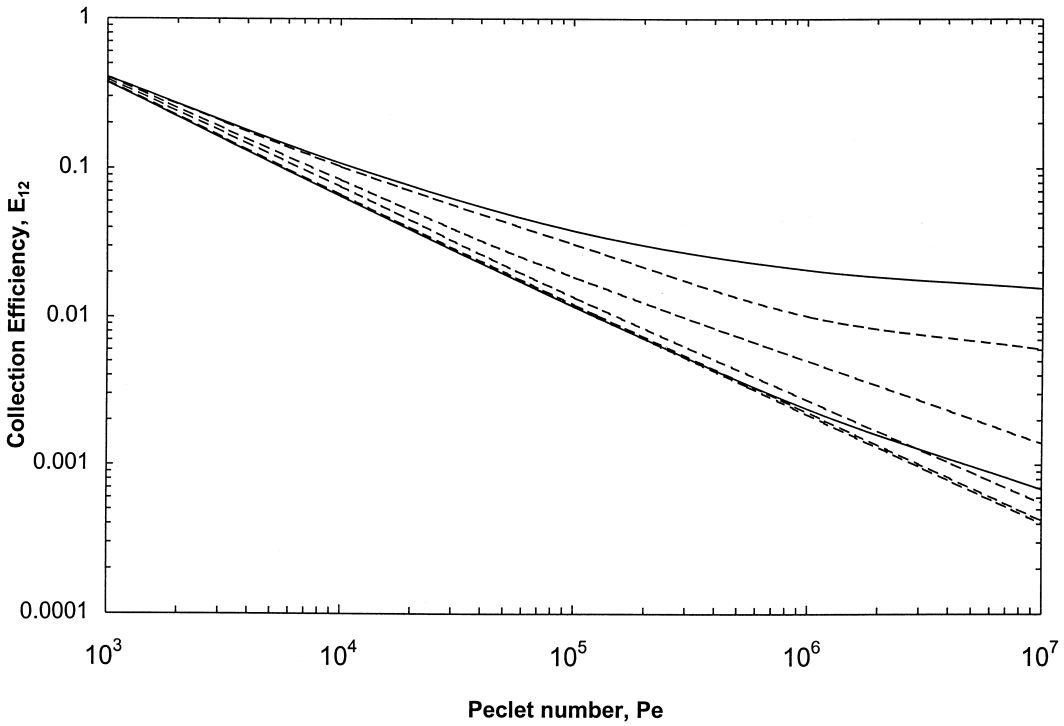

Fig. 8. Collection efficiency as a function of the bubble Péclet number for a fixed size ratio of $\lambda = 0.02$. The upper solid line is for bubbles with free surfaces, and the lower solid line is for rigid bubbles. The dashed lines are for $AP\mathrm{e}^{-1/4} = 0.1$, 1.0, 10, 100, and ∞ (top to bottom).

5. Concluding remarks

A mathematical model has been developed to calculate the collection efficiencies for which small bubbles capture microscopic suspended particles in the presence of a surface-active substance. Under conditions relevant to microflotation, the surfactant is considered to be insoluble in the bulk and, when the deviation from the average surfactant surface concentration on the surface of the bubble is small, Levich's theory of uniform retardation is employed for describing the interfacial motion of the bubble. The particle-bubble interaction was decomposed into axisymmetric and asymmetric contributions, and pairwise hydrodynamic mobility functions were calculated for different degrees of bubble surface retardation. The collection efficiencies were calculated using a trajectory analysis for motion induced by gravity only and by numerical solution of the parabolized Fokker–Planck equation for collisions under the combined effects of gravity and Brownian motion. Attractive van der Waals forces were included in the analysis.

The effect of the adsorbed surfactant on the surface mobility of the bubble is described by a retardation parameter which is the product of the Marangoni number and a surface Péclet

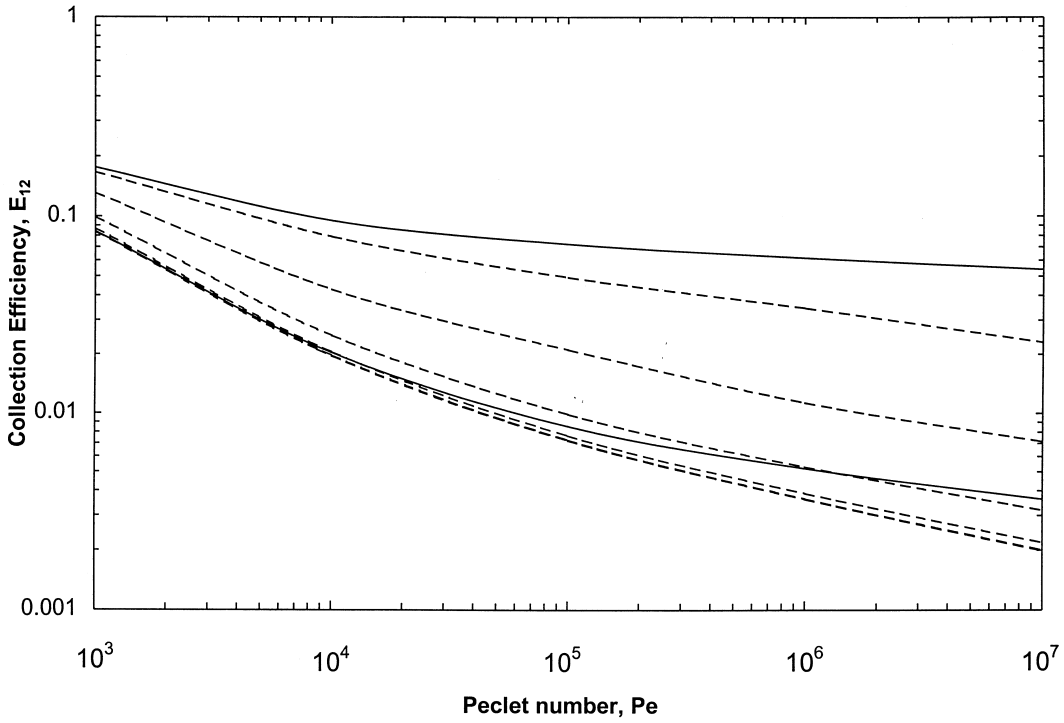

Fig. 9. Collection efficiency as a function of the bubble Péclet number for a fixed size ratio of $\lambda = 0.1$. The upper solid line is for a bubble with a free interface ($A = 0$), and the lower solid line is for a bubble with a rigid interface. The dashed lines are for $AP\mathrm{e}^{-1/4} = 1$, 10, 100, 1000, and ∞ (top to bottom).

number, $A = MaPe_s$. A wide range of values of this parameter may be encountered in practice (Ramirez and Davis, 1999). In general, a decrease in the surface mobility (through a higher value of A) brings about diminished flotation performance. The effect is less pronounced for smaller particles and bubbles, for which Brownian motion of the particles is strong. For larger bubbles and particles, convective and hydrodynamic effects have increased importance, and the effect of surface retardation is more dramatic, lowering the collection efficiencies by as much as an order of magnitude.

A minimum in the flotation collection efficiency versus particle size occurs for particles of approximately 1 μm diameter. This minimum represents a trade-off between higher capture rates with decreasing particle size due to increased Brownian motion, and reduced capture rates with decreasing particle size due to stronger hydrodynamic interactions causing the small particles to be swept past the rising bubble. The minimum shifts towards smaller particle sizes with increasing surface mobility (smaller values of A), because convective effects are then stronger due to the tangential sliding motion of the bubble interface.

Tangential motion of the surfactant-covered bubble interface occurs when in near-contact with a particle, even in the limit as $A \to \infty$. This sliding motion causes the transverse mobility

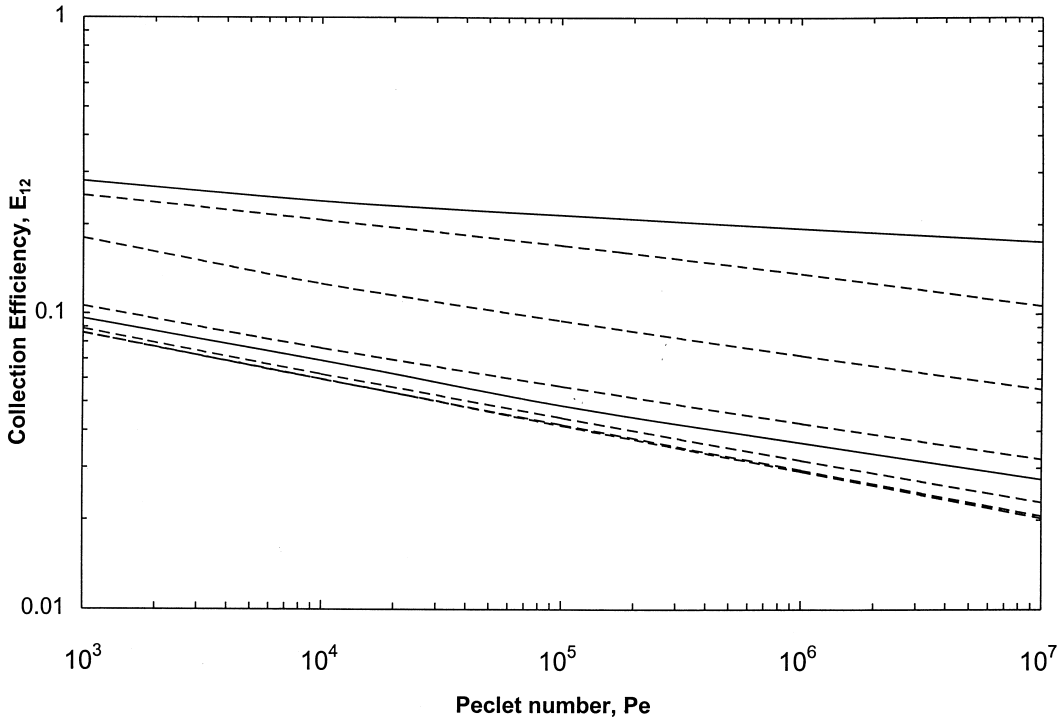

Fig. 10. Collection efficiency as a function of the bubble Péclet number for a fixed size ratio of $\lambda = 0.5$. The upper solid line is for a bubble with a free interface ($A = 0$), and the lower solid line is for a bubble with a rigid interface. The dashed lines are for $APe^{-1/4} = 1$, 10, 100, 1000, and ∞ (top to bottom).

functions for a bubble with surfactant in this limit to be higher than for a bubble with a rigid interface. As a result, the collection efficiency for large bubbles in the limit $A \rightarrow \infty$ is nearly two-fold lower than predicted from previous results (Loewenberg and Davis, 1994) for rigid bubbles of the same size.

Acknowledgements

This work was supported by NSF Grant CTS-9416702. The authors thank Prof. M. Loewenberg for forwarding them copies of the manuscripts by Blawzdziewicz et al. (1999) and Cristini et al. (1998) prior to their publication.

Appendix A. Axisymmetrical motion

Consider the bispherical coordinate system of Fig. 11, where

$$z = \frac{c\sinh \eta}{\cosh \eta - \cos \xi}, \tag{A1a}$$

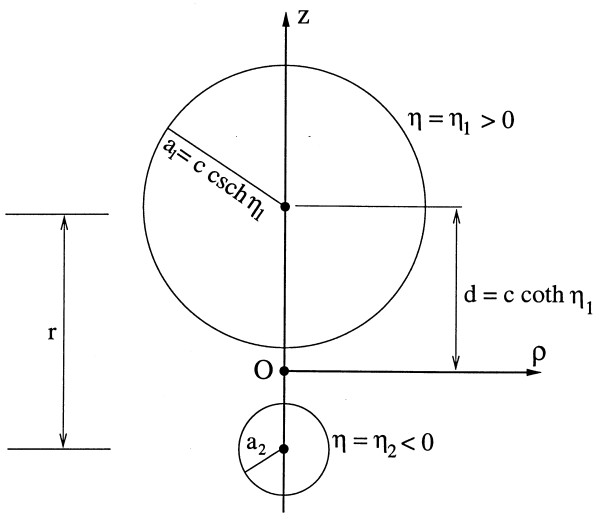

Fig. 11. Schematic for bispherical coordinate system used in the treatment of the axisymmetric problem.

$$\rho = \frac{c\sin\xi}{\cosh\eta - \cos\xi}. \tag{A1b}$$

The parameter c and the constants $\eta_1 > 0$ and $\eta_2 < 0$ may be determined for fixed bubble and particle radii (a_1 and a_2) through the expressions (Zinchenko, 1980)

$$\cosh\eta_1 = \frac{4(1-\lambda^2) + (1+\lambda^2)s^2}{4s(1+\lambda)}, \tag{A2a}$$

$$\lambda\sinh\eta_1 = \sinh\eta_2, \tag{A2b}$$

$$c = a_1\sinh\eta_1, \tag{A2c}$$

with $s = 2r/(a_1 + a_2)$ and $\lambda = a_2/a_1$. The interacting spherical bodies become coordinate surfaces when $\eta = \eta_1$ for the bubble and $\eta = \eta_2$ for the suspended particle.

The stream function for the flow field vanishing at infinity is given in bispherical coordinates by Jeffery (1912) as

$$\psi = \frac{c^2}{\sqrt{2}}(\cosh\eta - \mu)^{-3/2}\sum_{n=1}^{\infty} n(n+1)\Psi_n(\eta)Q_n(\mu), \tag{A3}$$

where $\mu = \cos\xi$, and $\Psi_n(\eta)$ is given in terms of the unknown coefficients A_n, B_n, C_n, and D_n by

$$\Psi_n(\eta) = A_n\cosh\big[(n-1/2)\eta\big] + B_n\sinh\big[(n-1/2)\eta\big] + C_n\cosh\big[(n+3/2)\eta\big] + D_n\sinh\big[(n+3/2)\eta\big], \tag{A4}$$

and $Q_n(\mu)$ is the $n+1$ order Gegenbauer polynomial related to the Legendre polynomials of degree $n+1$ and $n-1$ by $Q_n = (P_{n+1} - P_{n-1})/(2n+1)$.

Considerable simplification of the problem is made by considering the stream function for the relative fluid motion past the bubble (or particle), ψ^*. In this case, if a reference frame fixed to the moving body is used, the stream function is given by (Happel and Brenner, 1986)

$$\psi^* = \psi + \psi_\infty = \psi + \frac{1}{2} V_i \rho^2. \tag{A5}$$

Here, V_i is the velocity of the moving bubble ($i = 1$) or particle ($i = 2$) along the z-axis and ρ is the radial distance from the axis as defined in Fig. 11. The relative stream function can then be written as

$$\psi^* = \frac{c^2}{\sqrt{2}} (\cosh \eta - \mu)^{-3/2} \sum_{n=1}^{\infty} n(n+1) \Psi_n^*(\eta) Q_n(\mu), \tag{A6}$$

where

$$\Psi_n^*(\eta) = \Psi_n(\eta) + V_i \left[\frac{e^{-(n+3/2)|\eta|}}{2n+3} - \frac{e^{-(n-1/2)|\eta|}}{2n-1} \right], \quad i = 1 \text{ or } 2, \tag{A7}$$

The constants A_n,B_n,C_n, and D_n needed to completely define the stream function Ψ surrounding the bubble and particle can be found from the boundary conditions. The equations

$$\Psi_n^*(\eta_1) = 0, \tag{A8a}$$

$$\Psi_n^*(\eta_2) = 0, \tag{A8b}$$

result from the requirement of impenetrability of the flow at the surface (no-flux boundary condition). The condition of no slip on the solid particle requires that

$$\left. \frac{d\Psi_n^*}{d\eta} \right|_{\eta=\eta_2} = 0, \tag{A8c}$$

while the tangential stress balance (see Eq. (4)) yields the difference equation

$$\frac{-1}{\sinh \eta_1} \frac{(n-1)}{2n-1} \left. \frac{d^2 \Psi_{n-1}^*}{d\eta^2} \right|_{\eta=\eta_1} + \coth \eta_1 \left. \frac{d^2 \Psi_n^*}{d\eta^2} \right|_{\eta=\eta_1} - \frac{1}{\sinh \eta_1} \frac{(n+2)}{2n+3} \left. \frac{d^2 \Psi_{n+1}^*}{d\eta^2} \right|_{\eta=\eta_1}$$

$$= A \left. \frac{d\Psi_n^*}{d\eta} \right|_{\eta=\eta_1}, \tag{A8d}$$

where the function $\psi_n^*(\eta)$ is given by Eq. (A7).

The system of four equations (Eqs. (A8a)–(A8d)) for the unknown constants A_n and D_n can be reduced to a single second-order difference equation for one of the unknowns (say, A_n),

eventually resulting in a banded tridiagonal system for the set of coefficients from $n = 0$ to $n = N$ solved through a variant of the Thomas algorithm. The regularity of the flow field allows us to set the constants A_n, B_n, C_n, and D_n to zero at some large truncation bound N; only a straight-through run (in the direction of ascending n) is required (cf. Zinchenko, 1980), and the truncation bound, N, is determined automatically in the course of the calculations.

Stimson and Jefferey (1926) showed that the hydrodynamic forces acting on the spherical bodies along the axis parallel to their line of centers can be expressed in terms of the constants as

$$F_1 = -2\pi\mu a_1 c \sum_{n=1}^{\infty} n(n+1)(A_n + B_n + C_n + D_n), \tag{A9a}$$

$$F_2 = -2\pi\mu a_2 c \sum_{n=1}^{\infty} n(n+1)(A_n - B_n + C_n - D_n). \tag{A9b}$$

On the other hand, the forces along the line of centers can be expressed in terms of resistance coefficients Λ_{11}, Λ_{12}, Λ_{21}, and Λ_{22} as (Zinchenko, 1980)

$$F_1 = -6\pi\mu a_1 \left[\Lambda_{11}(V_1 - V_2) + \Lambda_{12} V_2\right], \tag{A10a}$$

$$F_2 = -6\pi\mu a_2 \left[\Lambda_{21}(V_2 - V_1) + \Lambda_{22} V_2\right]. \tag{A10b}$$

Eqs. (A9), and (A10), permit the calculation of the resistance coefficients from the stream-function constants; the former are related to the mobility functions $L(s)$ and $G(s)$ through

$$L(s) = \beta^* \frac{\Lambda_{22}}{\Lambda_{11}\Lambda_{22} + \Lambda_{12}\Lambda_{21}}, \tag{A11a}$$

$$G(s) = \frac{\beta^*}{\lambda + \beta^*} \frac{\Lambda_{12} + \lambda\Lambda_{22}}{\Lambda_{11}\Lambda_{22} + \Lambda_{12}\Lambda_{21}}, \tag{A11b}$$

where

$$\beta^* = \frac{A+2}{A+3}. \tag{A11c}$$

These relations apply only for the simplified case of $V_2^0 \ll V_1^0$ and negligible internal viscosity of the bubble.

Appendix B. Asymmetrical motion

Even though the method of bispherical coordinates is known to be highly efficient over a wide range of particle-to-bubble size ratios and to very small separations (Zinchenko, 1980), it is quite cumbersome to implement for the asymmetrical case of motion in the direction

perpendicular to the line of centers. Fortunately, we have found that the multipole expansion suffices for the current problem and gives rapid convergence. Consequently, the hydrodynamic problem of asymmetrical motion was solved by the method of multipole expansions, following the technique of Zinchenko (1982).

Consider two interacting spherical bodies using two right-handed spherical coordinate systems, (r_1,θ_1,φ_1) and (r_2,θ_2,φ_2), as shown in Fig. 12x. The angle φ_i corresponds to positive rotation about the z_i-axis, while $\varphi_i = 0$ defines the half plane contained by the $x_i > 0$-axis and the line of centers. The spatial variables are made non-dimensional by choosing the center-to-center distance ℓ as the length scale. The velocity field in the region between the spheres can be written in the form, $\boldsymbol{v} = \boldsymbol{v}^1_- + \boldsymbol{v}^2_-$. Here, each field $\boldsymbol{v}^i_-$ satisfies the Stokes equations, is regular everywhere outside of the sphere of radius a_i and vanishes at infinity. These unknown fields can be represented in terms of Lamb's general solution of Stokes equations as (Lamb, 1945)

$$\boldsymbol{v}^i_- = \sum_{n=1}^{\infty}\left[\nabla\times\left(\boldsymbol{r}_i\chi^i_{-(n+1)}\right) + \nabla\Phi^i_{-(n+1)} + \frac{(n-2)r_i^2\nabla p^i_{-(n+1)}}{2n(2n-1)} - \frac{(n+1)\boldsymbol{r}_i p^i_{-(n+1)}}{n(2n-1)}\right], \tag{B1}$$

where the decaying harmonic functions $\chi^i_{-(n+1)}$, and $\Phi^i_{-(n+1)}$ and $p^i_{-(n+1)}$ are given by (Zinchenko, 1982)

$$p^i_{-(n+1)} = r_i^{-(n+1)}P^1_n(\cos\theta_i)A^i_{-(n+1)}\cos\varphi_i, \tag{B2a}$$

$$\Phi^i_{-(n+1)} = r_i^{-(n+1)}P^1_n(\cos\theta_i)B^i_{-(n+1)}\cos\varphi_i, \tag{B2b}$$

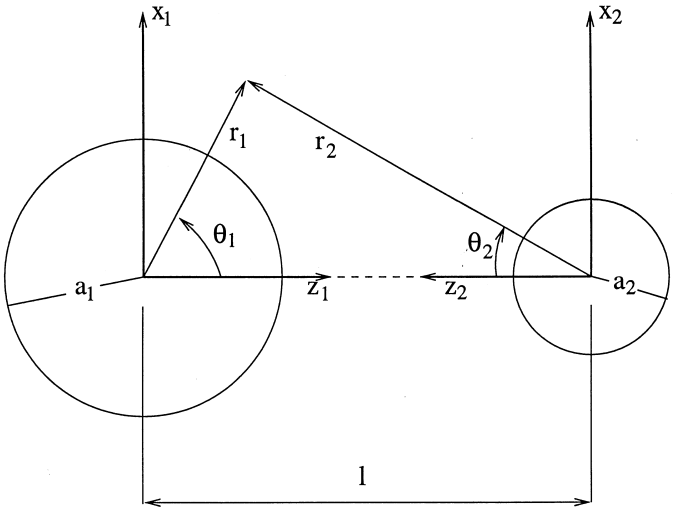

Fig. 12. Schematic of coordinate systems used in the treatment of the asymmetric problem.

$$\chi^{i}_{-(n+1)} = r_i^{-(n+1)} P^1_n(\cos\theta_i) C^{\,i}_{-(n+1)} \sin\varphi_i. \tag{B2c}$$

Here, $A^i_{-(n+1)}$, $B^i_{-(n+1)}$, and $C^{\,i}_{-(n+1)}$ are unknown coefficients, while P^1_n is the associated Legendre function.

In order to satisfy the boundary conditions on the bubble and particle surfaces, each field, v^i_-, should be reexpanded in the vicinity of the other sphere ($i+1$; the indices i, $i+1$ are reduced by module 2) in Lamb's regular form,

$$\boldsymbol{v}^{i+1}_{+} = \sum_{n=1}^{\infty}\left[\nabla\times\left(\boldsymbol{r}_{i+1}\chi^{i+1}_n\right) + \nabla\Phi^{i+1}_n + \frac{(n+3)r^2_{i+1}\nabla p^{i+i}_n}{2(n+1)(2n+3)} - \frac{n r_{i+1} p^{i+i}_n}{(n+1)(2n+3)}\right], \tag{B3}$$

with the growing harmonic functions χ^{i+1}_n, Φ^{i+1}_n and p^{i+1}_n given by (Zinchenko, 1982)

$$p^{i+1}_n = r^n_{i+1} P^1_n(\cos\theta_{i+1}) A^{i+1}_n \cos\varphi_{i+1}, \tag{B4a}$$

$$\Phi^{i+1}_n = r^n_{i+1} P^1_n(\cos\theta_{i+1}) B^{i+1}_n \cos\varphi_{i+1}, \tag{B4b}$$

$$\chi^{i+1}_n = r^n_{i+1} P^1_n(\cos\theta_{i+1}) C^{\,i+1}_n \sin\varphi_{i+1}. \tag{B4c}$$

The necessary relations for reexpansion of the velocity fields are (Zinchenko, 1982)

$$A^{i+1}_n = \sum_{m=1}^{\infty} g^m_n A^i_{-(m+1)}, \tag{B5}$$

$$B^{i+1}_n = \sum_{m=1}^{\infty}\frac{A^i_{-(m+1)}}{m(2m-1)}\left[\frac{(n-1)\big((m-2)(n-1)-(m+1)\big)}{n(2n-1)} g^m_{n-1} - \frac{m-2}{2} g^m_n\right] + g^m_n B^i_{-(m+1)} + \frac{m}{n+1} C^{\,i}_{-(m+1)}, \tag{B6}$$

$$C^{\,i+1}_n = \sum_{m=1}^{\infty}\frac{g^m_n}{mn(n+1)} A^i_{-(m+1)} + \frac{m}{n+1} g^m_n C^{\,i}_{-(m+1)}, \tag{B7}$$

where

$$\frac{g^m_n = (n+m)!}{(m-1)!(n+1)!}. \tag{B8}$$

As with the axisymmetric case (Appendix A), it is convenient to consider the relative dimensionless flow velocity, $\boldsymbol{v}^* = \boldsymbol{v} - \boldsymbol{V}_1$, in the vicinity of the bubble (sphere 1), where $\boldsymbol{V}_1 = (V_1,0,0)$ is its dimensionless translational velocity vector given by (Happel and Brenner, 1986) and

$$\boldsymbol{v}_1^* = \sum_{n=-\infty}^{\infty}\left[\nabla\times\left(\boldsymbol{r}_1\chi_n^1\right)+\nabla\tilde{\Phi}_n^1+\frac{(n+3)r_1^2\nabla p_n^1}{2(n+1)(2n+3)}-\frac{n\boldsymbol{r}_1 p_n^1}{(n+1)(2n+3)}\right],\quad n\neq 1, \tag{B9}$$

where $\tilde{\Phi}_n^1=\Phi_n^1-\delta_{n,1}\boldsymbol{V}_1\boldsymbol{r}_1\sin\theta_1\cos\varphi_1$ and $\delta_{n,1}$ is the Kronecker delta function. For the normal component of $\boldsymbol{v}^*$ on the surface of the bubble, the relation (Happel and Brenner, 1986)

$$\boldsymbol{v}^*\cdot\boldsymbol{e}_r=\sum_{n=-\infty}^{\infty}\left[\frac{n}{r_1}\tilde{\Phi}_n^1+\frac{nr_1p_n^1}{2(2n+3)}\right] \tag{B10}$$

can be used, with $\boldsymbol{e}_r$ being the outward unit normal for sphere 1. Grouping together the terms with n and $-(n+1)$, we obtain from Eq. (B10)

$$\boldsymbol{v}^*\cdot\boldsymbol{e}_r=\sum_{n=1}^{\infty}\left[\frac{n}{2(2n+3)}r_1p_n^1+\frac{n}{r_1}\tilde{\Phi}_n^1-\frac{n+1}{2(2n-1)}r_1p_{-(n+1)}^1-\frac{n+1}{r_1}\Phi_{-(n+1)}^1\right]. \tag{B11}$$

The condition of no-flux through the bubble surface ($\boldsymbol{v}^*\cdot\boldsymbol{e}_r=0$) then can be written, after using Eqs. (B2a,b) and (B4a,b) for the spherical harmonics, as

$$\frac{A_n^1 n\alpha_1^{n+1}}{2(2n+3)}+\tilde{B}_n^1 n\alpha_1^{n-1}-\frac{A_{-(n+1)}^1(n+1)\alpha_1^{-n}}{2(2n-1)}-B_{-(n+1)}^1(n+1)\alpha_1^{-(n+2)}=0, \tag{B12}$$

with $\tilde{B}_n^1=B_n^1$ for $n\neq 1$, $\tilde{B}_1^1=B_1^1-\boldsymbol{V}_1$, and $\alpha_1=a_1/\ell$.

A second relation results from the equation of conservation of surfactant at the surface of the bubble, Eq. (4), which may be written in terms of the volumetric divergence as (Happel and Brenner, 1986)

$$\nabla\cdot\left[\frac{A}{\alpha_1}v^*+\boldsymbol{\Pi}\right]-\frac{1}{r^2}\frac{\partial}{\partial r}\left[r^2\left(\frac{A}{\alpha_1}\boldsymbol{v}_1^*+\boldsymbol{\Pi}\right)\cdot\boldsymbol{e}_r\right]=0. \tag{B13}$$

The stress vector acting across the surface of the bubble in terms of the spherical harmonics is (Happel and Brenner, 1986)

$$\begin{aligned}\boldsymbol{\Pi}=\frac{1}{r_1}\sum_{v=-\infty}^{\infty}\Bigg[&(v-1)\nabla\times\left(\boldsymbol{r}_1\chi_v^1\right)\\&+2(v-1)\nabla\tilde{\Phi}_v^1-\frac{\left(2v^2+4v+3\right)}{(v+1)(2v+3)}\boldsymbol{r}_1\pi_v^1+\frac{n(n+2)}{(n+1)(2n+3)}r_1^2\nabla p_n^1\Bigg],\quad n\neq -1.\end{aligned} \tag{B14}$$

Using Eq. (B9) for the dimensionless relative fluid velocity, v^*, and Eq. (B14) for the dimensionless stress vector, $\boldsymbol{\Pi}$, evaluated at $r_1=\alpha_1$, we obtain from Eq. (B13) that

$$\sum_{n=-\infty}^{\infty}\left[\left(\frac{n^2(n+2)}{2n+3}+A\frac{n(n+1)}{2(2n+3)}\right)\frac{p_n^1}{\alpha_1}+\left(2(n^2-1)n+A\frac{n(n-1)}{r_1^2}\right)\frac{\tilde{\Phi}_n^1}{\alpha_1^3}\right]=0. \tag{B15}$$

Grouping together the terms with n and $-(n+1)$ in Eq. (B15) yields

$$\sum_{n=1}^{\infty}\Bigg\{\left[\frac{n^2(n+2)}{2n+3}+A\frac{n(n+1)}{2(2n+3)}\right]\frac{p_n^1}{\alpha_1}+\left[2(n^2-1)n+An(n-1)\right]\frac{\tilde{\Phi}_n^1}{\alpha_1^3}$$

$$+\left[\frac{(n-1)(n+1)^2}{2n-1}-A\frac{n(n+1)}{2(2n-1)}\right]\frac{p_{-(n+1)}^1}{\alpha_1} \tag{B16}$$

$$-\left[2n(n+2)(n+1)-A(n+1)(n+2)\right]\frac{\Phi_{-(n+1)}^1}{\alpha_1^3}\Bigg\}=0.$$

When the harmonic functions are represented by Eqs. (B2) and (B4), we obtain

$$\left[\frac{n^2(n+2)}{2n+3}+A\frac{n(n+1)}{2(2n+3)}\right]\alpha_1^{n-1}A_n^1+\left[\frac{(n-1)(n+1)^2}{2n-1}-A\frac{n(n+1)}{2(2n-1)}\right]\alpha_1^{-(n+2)}A_{-(n+1)}^1+$$

$$\left[2(n^2-1)n+An(n-1)\right]\alpha_1^{n-3}\tilde{B}_n^1-\left[2n(n+2)(n+1)-A(n+1)(n+2)\right]\alpha_1^{-(n+4)}B_{-(n+1)}^1=0. \tag{B17}$$

The combination of Eqs. (B12) and (B17) yields the following relationships between the expansion coefficients:

$$A_{-(n+1)}^1=\frac{n(2n-1)}{2(2n+1-A)(n+1)}\left[A\alpha_1^{2n+1}A_n^1-2\left[(2n+1)(2-A)\right]\alpha_1^{2n-1}\tilde{B}_n^1\right], \tag{B18}$$

$$B_{-(n+1)}^1=\frac{n}{2(2n+1-A)(n+1)}\left[\frac{(2n+1)(2+A)}{2(2n+3)}\alpha_1^{2n+3}A_n^1+A(2n-1)\alpha_1^{2n+1}\tilde{B}_n^1\right]. \tag{B19}$$

A third equation comes from writing (Happel and Brenner, 1986)

$$(\nabla\times\boldsymbol{\Pi})\cdot\hat{\boldsymbol{e}}_r=\frac{1}{r_1\sin\theta_1}\left[\frac{\partial}{\partial\theta_1}\left[\sin\theta_1(\boldsymbol{\Pi})_{\varphi_1}\right]-\frac{\partial}{\partial\varphi_1}(\boldsymbol{\Pi})_{\theta_1}\right], \tag{B20}$$

where $(\boldsymbol{\Pi})_{\varphi_1}$ and $(\boldsymbol{\Pi})_{\theta_1}$ are the components of the dimensionless stress vector acting across the bubble surface in the two mutually perpendicular tangential directions. From our discussion of Section 2, it is seen that

$$(\boldsymbol{\Pi})_{\varphi_1}=-Ma\left(\nabla_s\Gamma'\right)_{\varphi_1}=-Ma\frac{1}{r_1\sin\theta_1}\frac{\partial\Gamma'}{\partial\varphi_1}, \tag{B21a}$$

$$(\boldsymbol{\Pi})_{\theta_1}=-Ma\left(\nabla_s\Gamma'\right)_{\theta_1}=-Ma\frac{1}{r_1}\frac{\partial\Gamma'}{\partial\theta_1}. \tag{B21b}$$

Substitution of Eq. (B21) into Eq. (B20) results in $(\nabla\times\boldsymbol{\Pi}_r)\cdot\hat{\boldsymbol{e}}=0$, which, when combined with Eq. (B14) for the stress vector and grouping together the terms with n and $-(n+1)$, results in

$$\sum_{n=1}^{\infty}(n-1)(n+1)n\chi_n^1-(n+2)(n+1)n\chi_{-(n+1)}^1=0. \tag{B22}$$

Using Eqs. (B2c) and (B4c) and evaluating at $r_1=\alpha_1$, yields

$$C_{-(n+1)}^{1}-\frac{(n-1)\alpha_1^{2n+1}}{(n+2)}C_n^1=0. \tag{B23}$$

The no-flux boundary condition on the suspended particle,

$$\frac{A_n^2 n\alpha_2^{n+1}}{2(2n+3)}+\tilde{B}_n^2 n\alpha_2^{n-1}+\frac{A_{-(n+1)}^2(n+1)\alpha_2^{-n}}{2(2n-1)}-B_{-(n+1)}^2(n+1)\alpha_2^{-(n+2)}=0, \tag{B24}$$

with $\tilde{B}_n^2=B_n^2$ for $n\neq 1$ and $\tilde{B}_1^2=B_1^2-V_1$, is obtained in analogous fashion as for the surface of the bubble discussed earlier.

On the other hand, it is seen from the no-slip boundary condition that

$$\left[\nabla\times(\boldsymbol{v}-\boldsymbol{V}_2-\boldsymbol{\Omega}_2\times r_2)\right]\cdot\boldsymbol{e}_r=0, \tag{B25}$$

where the particle dimensionless translational velocity is $\boldsymbol{V}_2=(V_2,0,0)$ and its velocity of rotation is $\boldsymbol{\Omega}_2=(0,\Omega_2,0)$. Using

$$\boldsymbol{v}-\boldsymbol{V}_2=\sum_{n=-\infty}^{\infty}\left[\nabla\times\left(\boldsymbol{r}_2\chi_n^2\right)+\nabla\tilde{\Phi}_n^2+\frac{(n+3)r_2^2\nabla p_n^2}{2(n+1)(2n+3)}-\frac{n\boldsymbol{r}_2 p_n^2}{(n+1)(2n+3)}\right],\quad n\neq -1, \tag{B26}$$

where $\tilde{\Phi}_n^2=\Phi_n^2-\delta_{n,1}V_2 r_2\sin\theta_2\cos\varphi_2$ the following relation results (Happel and Brenner, 1986):

$$\left[\nabla\times(\boldsymbol{v}-\boldsymbol{V}_2-\boldsymbol{\Omega}_2\times\boldsymbol{r}_2)\right]\cdot\boldsymbol{e}_r=\sum_{n=-\infty}^{\infty}n(n+1)\chi_n^2, \tag{B27}$$

which, when the terms with n and $-(n+1)$ are grouped, becomes

$$\sum_{n=1}^{\infty}n(n+1)\chi_n^2+n(n+1)\chi_{-n+1}^2=0, \tag{B28}$$

with $\tilde{\chi}_n^2=\chi_n^2-\Omega_2 r_2\sin\theta_2\sin\phi_2$. Using Eqs. (B2c) and (B4c) for the harmonic function, and evaluating at $r_2=\alpha_2$, we obtain

$$C_{-(n+1)}^{2}+\alpha_2^{2n+1}\tilde{C}_n^2=0. \tag{B29}$$

A third relation is obtained from the continuity equation applied at the surface of the particle:

$$\nabla\cdot\boldsymbol{v}_2^*=\frac{1}{r_2^2}\frac{\partial}{\partial r_2}\left[r_2^2 v_{r_2}^*\right]+\nabla_s\cdot v^*=0, \tag{B30}$$

where the relative fluid velocity with respect to the particle is $\boldsymbol{v}^*=\boldsymbol{v}-\boldsymbol{V}_2-\boldsymbol{\Omega}_2\times\boldsymbol{r}_2$, $v_{r_2}^*$ is the component of this velocity in the direction normal to the particle surface, and ∇_s is applied along the surface. As a consequence of the no-slip condition, the contribution of the surface

divergence term in Eq. (B30) is zero, and thus we are left with

$$r_2 \frac{\partial v^*_{r_2}}{\partial r_2} = 0. \tag{B31}$$

Using the expression (Happel and Brenner, 1986)

$$r_2 \frac{\partial v^*_{r_2}}{\partial r_2} = \sum_{n=-\infty}^{\infty} \left[\frac{n(n-1)}{r_2} \tilde{\Phi}^2_n + \frac{n(n+1) r_2 p^2_n}{2(2n+3)} \right], \tag{B32}$$

and grouping the terms with n and $-(n+1)$, results in

$$\sum_{n=1}^{\infty} \left[\frac{n(n-1)}{r_2} \tilde{\Phi}^2_n + \frac{(n+1)(n+2)}{r_2} \Phi^2_{-(n+1)} + \frac{n(n+1)}{2(2n+3)} r_2 p^2_n - \frac{n(n+1)}{2(2n-1)} r_2 p^2_{-(n+1)} \right] = 0. \tag{B33}$$

Using Eqs. (B2) and (B4) for the remaining harmonic functions in Eq. (B33), one obtains

$$\begin{aligned} & n(n-1)\alpha_2^{n-1} \tilde{B}^2_n + \frac{n(n+1)}{2(2n+3)} \alpha_2^{n+1} A^2_n \\ & \quad + (n+1)(n+2)\alpha_2^{-(n+2)} B^2_{-(n+1)} - \frac{n(n+1)}{2(2n-1)} \alpha_2^{-n} A^2_{-n+1} = 0, \end{aligned} \tag{B34}$$

with $\tilde{B}^2_n$ as defined earlier. The combination of Eqs. (B24) and (B34) yields the relations,

$$A^2_{-(n+1)} = -\frac{n(2n-1)}{2(n+1)} \left[\alpha_2^{2n+1} A^2_n + 2(2n+1)\alpha_2^{2n-1} \tilde{B}^2_n \right], \tag{B35}$$

$$B^2_{-(n+1)} = -\frac{n}{2(2n+3)(n+1)} \left[\frac{(2n+1)}{2} \alpha_2^{2m+3} A^2_n + (2n-1)(2n+3)\alpha_2^{2n+1} \tilde{B}^2_n \right]. \tag{B36}$$

Eqs. (B5)–(B8), (B18), (B19), (B23), (B29), (B35) and (B36) permit the calculation of the constants A^i_n, B^i_n and C^i_n. The calculation is started by arbitrarily setting A^2_n, B^2_n and C^2_n to zero for $n \neq 1$. For $n = 1$, the constants A^1_2 and $\tilde{B}^2_1$ are calculated from Eqs. (B35) and (B36), since A^2_{-2} is known through specification of the force acting on the particle (Happel and Brenner, 1986), $\boldsymbol{F}_2 = -4\pi\mu\nabla(r_2^3 p^2_{-2})$. Furthermore, since there is no net applied torque, $\boldsymbol{T}_2 = -8\pi\mu\nabla(r_2^3 \chi^2_{-2}) = 0$, we conclude that $C^2_{-2} = 0$. Eqs. (B29), (B35) and (B36) are used to calculate the coefficients $A^2_{-(n+1)}$, $B^2_{-(n+1)}$ and $C^2_{-(n+1)}$. The first reexpansion is effected by using Eqs. (B5)–(B8), which yields the coefficients A^1_n, B^1_n and C^1_n, after which (B18), (B19) and (B23) are used for calculating $A^1_{-(n+1)}$, $B^1_{-(n+1)}$ and $C^1_{-(n+1)}$ (where, analogously to the case of the particle, A^1_{-2} is known and B^1_n and A^1_1 are calculated from Eqs. (B18) and (B19) with $n = 1$). The reexpansion relations are then used for recalculating the coefficients A^2_n, B^2_n and C^2_n. The procedure is repeated until convergence of the terms $B^2_1 - \tilde{B}^2_1 = V^{\perp}_2$ and $B^1_1 - \tilde{B}^1_1 = V^{\perp}_1$, which represent the dimensionless translational velocities of the particle and bubble, respectively, in the direction perpendicular to their line of centers.

Once the bubble and particle velocities are known, the mobility coefficients can easily be

obtained from their definitions (Batchelor, 1982):

$$M(s) = \frac{V_1^{\perp} - V_2^{\perp}}{V_1^0 - V_2^0} \tag{B37}$$

$$H(s) = \frac{V_1^{\perp} - V_2^{\perp}}{D_{12}^0/kT} \tag{B38}$$

where the far-field relative velocity is given by Eq. (9) and the far-field relative diffusivity is given by Eq. (10)

References

Agrawal, S., Wasan, D., 1979. The effect of interfacial viscosities on the motion of drops and bubbles. Chem. Eng. J 18, 215–223.

Batchelor, G.K., 1982. Sedimentation in a dilute polydisperse system of interacting spheres. Part I: general theory. J. Fluid Mech 119, 379–408.

Blawzdziewicz, J., Wajnryb, E., Loewenberg, M., 1999. Hydrodynamic interactions and collision efficiencies of spherical drops covered with an incompressible surfactant film. J. Fluid Mech.395, 29–59.

Brunn, P.O., Isemin, D., 1984. Dimensionless heat-mass transfer coefficients for forced convection around a sphere: a good general low Reynolds number correlation. Int. J. Heat Mass Transfer 27, 2339–2345.

Cristini, V., Blawzdziewicz, J., Loewenberg, M., 1998. Near-contact motion of surfactant-covered spherical drops. J. Fluid Mech 366, 259–287.

Cuenot, B., Magnaudet, J., Spennato, B., 1997. The effects of slightly soluble surfactants on the flow around a spherical bubble. J. Fluid Mech 339, 25–53.

Frumkin, A., Levich, V.G., 1947. O vliyanii poverkhnostno-aktivnikh veshestv na dvizhenie na granitse zhidkikh sred. Zhur. Fizic. Khimii 21, 1183–1204.

Gaudin, A.M., 1957. Flotation, 2nd ed. McGraw-Hill, NY.

Griffith, R., 1962. The effect of surfactants on the terminal velocity of drops and bubbles. Chem. Eng. Sci 17, 1057–1070.

Happel, J., Brenner, H., 1986. Low Reynolds Number Hydrodynamics. Martinus Nijhoff Publishers, Boston, MA.

Harper, J.F., 1988. The near stagnation region of a bubble rising steadily in a dilute surfactant solution. Q. J. Mech. Appl. Math 41, 204–213.

Ho, N.F., Higuchi, W.I., 1968. Preferential aggregation and coalescence in netero dispersed system. J. Pharm. Sci 57, 436–442.

Holbrook, J.A., LeVan, M.D., 1983. Retardation of droplet motion by surfactants. Part I: theoretical development asymptotic solutions. Chem. Eng. Commun 20, 191–207.

Jeffery, G.B., 1912. On a form of the solution of Laplace/s equation suitable for problems relating to two spheres. Proc. Roy. Soc A87, 109–120.

Kawase, Y., Ulbrecht, J.J., 1982. The effect of surfactant on terminal velocity of and mass transfer from a fluid sphere in a non-Newtonian fluid. Can. J. Chem. Eng 60, 87–93.

Lamb, H., 1990. Hydrodynamics, 6th ed. Dover, New York.

Lerner, L., Harper, J.F., 1991. Stokes flow past a pair of stagnant-cap bubbles. J. Fluid Mech 232, 167–190.

Levich, V, 1962. Physicochemical Hydrodynamics. Prentice-Hall, Englewood Cliffs, NJ.

Lochiel, A.C., 1965. The influence of surfactants on mass transfer around spheres. Can. J. Chem. Eng 43, 40–44.

Loewenberg, M., Davis, R.H., 1994. Flotation rates of fine spherical particles and droplets. Chem. Eng. Sci 49, 3923–3941.

Ramirez, J.A., Davis, R.H., 1999. Mass transfer to a surfactant-covered bubble. AIChE J 45, 1355–1358.

Ramirez, J.A., Zinchenko, A., Loewenberg, M.L., Davis, R.H., 1999. The flotation rates of fine spherical particles under convective and Brownian motion. Chem. Eng. Sci 54, 149–157.

Sadhal, S., Johnson, R., 1983. Stokes flow past bubbles and drops partially coated with thin films. J. Fluid Mech 126, 237–250.

Saville, D., 1973. The effect of interfacial tension gradients and droplet behaviour. Chem. Eng. J 5, 251–259.

Schenkel, J.H., Kitchener, J.A., 1960. A test of the Derjaguin-Verwey-Overbeek theory with a colloidal suspension. Trans. Farad. Society 56, 161–173.

Stimson, M., Jefferey, G.B., 1926. The motion of two spheres in a viscous fluid. Proc. Roy. Soc A111, 110–116.

Wasserman, M., Slattery, J., 1969. Creeping flow past a fluid globule when a trace of surfactant is present. AIChE J 15, 533–541.

Yang, S.-M., Han, S.P., Hong, J.J., 1995. Capture of small particles on a bubble collection by Brownian diffusion and interception. J. Colloid Interf. Sci 169, 125–134.

Zabel, T., 1984. Flotation in water treatment. In: Ives, K.J. (Ed.), The Scientific Basis of Flotation. NATO ASI Series, Series E: Applied Sciences — No. 75, 349. Martinus Nijhoff Publishers, The Hague, NL.

Zhang, X., Davis, R.H., 1991. The rate of collisions due to Brownian or gravitational motion of small drops. J. Fluid Mech 230, 479–504.

Zinchenko, A.Z., 1980. The slow asymmetric motion of two drops in a viscous medium. Prikl. Matem. Mekhan 44, 30–37.

Zinchenko, A.Z., 1982. Calculation of the effectiveness of gravitational coagulation of drops with allowance for internal circulation. Prikl. Matem. Mekhan 46 (1), 58–65.

Zinchenko, A.Z., Davis, R.H., 1994. Gravity-induced coalescence of drops at arbitrary Péclet numbers. J. Fluid Mech 280, 119–148.